IEEE Photonics Journal
An IEEE Photonics Society Publication

A Novel Eigenvalue Algorithm for the Complex Band Structure and Eigenmodes of Plasmonic Crystals

Volume 8, Number 2, April 2016

Hui Wang
Wei E. I. Sha, Member, IEEE
Zhixiang Huang
Xianliang Wu

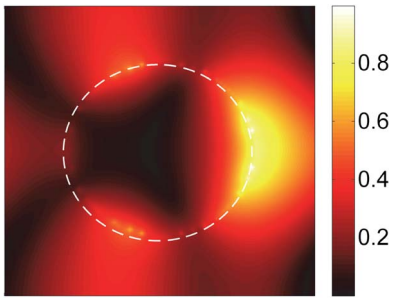

DOI: 10.1109/JPHOT.2016.2536939
1943-0655 © 2016 IEEE

A Novel Eigenvalue Algorithm for the Complex Band Structure and Eigenmodes of Plasmonic Crystals

Hui Wang,[1,2] Wei E. I. Sha,[3] *Member, IEEE*, Zhixiang Huang,[1] and Xianliang Wu[1,2]

[1]Key Laboratory of Intelligent Computing & Signal Processing, Ministry of Education, Anhui University, Hefei 230039, China
[2]School of Electronic and Information Engineering, Hefei Normal University, Hefei 230601, China
[3]The University of Hong Kong, Pokfulam, Hong Kong

DOI: 10.1109/JPHOT.2016.2536939

Manuscript received February 19, 2016; accepted February 26, 2016. Date of publication March 2, 2016; date of current version April 1, 2016. This work was supported in part by the Seed Project Funding of Hong Kong University under Grant 201211159147; by the University Grants Committee of Hong Kong under Grant AoE/P-04/08 and Special Equipment Grant SEG HKU09; by the National Natural Science Foundation of China under Grant 51277001, Grant 61201122, Grant 61471001, and Grant 61301062; by the Natural Science Foundation of Anhui Province under Grant 1508085JGD03, Grant 1508085QF130, Grant KJ2015A202, and Grant KJ2015A292; and by the Scientific Research Starting Foundation for New Teachers of Hefei Normal University (No. 2015rcjj05). Corresponding authors: W. E. I. Sha and Z. Huang (e-mail: wsha@eee.hku.hk; zxhuang@ahu.edu.cn).

Abstract: The influence of ohmic (metallic) loss on the complex band structure (BS) and eigenmodes of 2-D plasmonic crystals is investigated. With the help of wave equations and periodic boundary conditions, a finite-difference-based eigenvalue algorithm is proposed to model the plasmonic crystals with arbitrarily lossy and dispersive materials. Given a frequency of interests, the algorithm solves one complex Bloch wavenumber as the eigenvalue via fixing another. Most importantly, the developed eigenvalue analysis could expand the bulk excitation solution with eigenmodes, which satisfies the generalized phase (momentum) matching condition. For a TE polarization with H_z field, the ohmic loss strongly affects the BS and eigenmodes at plasmonic resonance frequencies. Both the fast oscillation of a dispersion curve and strong field confinement of eigenmodes are damped due to the high ohmic loss. For a TM polarization with E_z field, the introduction of ohmic loss twists the vertical dispersion curve at the bandgap and breaks the symmetry of the eigenmodes. For both polarizations, the high ohmic loss lowers the quality factor of the eigenmodes. This paper offers a fundamental and important eigenvalue analysis for designing lossy and dispersive plasmonic crystals.

Index Terms: Complex band structure, plasmonic crystals, bandgap.

1. Introduction

Over the past few years, remarkable progress has been made in artificially structured materials, such as photonic crystals and metamaterials, because of their extraordinary optical properties to control and manipulate light [1], [2]. The investigation of optical properties of such a periodic structure relies on its band diagram (structure) and eigenmodes. Regarding the conventional numerical method [1], [3] for calculating the BS and eigenmodes, one first established the partial differential equation characterizing the geometry, material composition, and periodic (Bloch) boundary condition of a unit cell. Then, the continuous eigenequation is converted into an

algebraic eigenvalue problem with a frequency ω as the eigenvalue for a fixed Bloch wave vector $\mathbf{k}$, where the dispersion relation $\omega = \omega(\mathbf{k})$ is obtained. Considering non-dispersive materials, the eigensystem reduces to a standard linear eigenvalue problem that can be solved by standard linear eigenvalue solvers [4], [5].

Although most of previous studies focused on photonic crystals composed of frequency-independent permittivity, currently there are more interests in photonic crystals with dispersive materials, and particularly in plasmonic crystals showing unprecedented ability to confine optical energy in deep subwavelength scales. The strong optical confinement is due to a coherent interaction of electromagnetic fields with free electrons of metals leading to surface plasmon resonance and local plasmon resonance [6], [7]. The forward and backward surface plasmon waves interfering with each other induce the plasmonic band gap (PBG) and plasmonic band edge (PBE) [8], [9]. Meanwhile, the Bragg backscattering from individual metallic scatterers also opens up photonic band gaps [10], [11]. Because of a pronounced near-field enhancement, plasmonic crystals find versatile interesting applications in fields of solar cells [12]–[14], optical detection [15], [16], subwavelength waveguides [17], sensing [18], etc.

Just like photonic crystals, the BS and eigenmodes of plasmonic crystals are essential to understand relevant physical effects and design novel optical devices. However, a lot of computational challenges arise. On one hand, a dense mesh generation is required at the metal-dielectric interface owing to the highly localized nature of plasmons. On the other hand, metals at the optical regime are very dispersive and lossy materials with the frequency-dependent permittivity. Consequently, the eigensystem for plasmonic crystals is no longer a standard linear eigenvalue problem but a nonlinear eigenvalue one, where the poles or zeros of a function or a determinant on a complex plane must be found [19]. Methods using nonlinear iterative solvers are time-consuming while approaches taking the Bloch wave vector $\mathbf{k}$ instead of the frequency ω to be eigenvalues are numerically practical and favorable. In other words, the intractable nonlinear eigenvalue problem could be recasted into a tractable quadratic eigenvalue problem (QEP) where the wave vector is a function of frequency $(\mathbf{k} = \mathbf{k}(\omega))$. In the literatures, Raman [20] solved the Hermitian QEP. Unfortunately, extending the method to handle arbitrary permittivity with N-pole Lorenz model is nontrivial. The Dirichlet-to-Neumann wave vector eigenequation [21] converted QEP into a generalized eigenvalue problem of twice the size, which can be easily solved. Luo Ma *et al.* [22] used the spectral element method to calculate the band structures of 2-D and 3-D photonic crystals consisting of dispersive anisotropic and metallic materials. They found the spectral element method (SEM) have spectral accuracy with the error decreasing exponentially with the order of basis functions compared to the conventional finite element and finite difference methods. Full-wave finite element [23], [24] also overcome the difficulty and can simulate arbitrary material compositions, but they were essential QEPs with a large memory and computational complexity due to augmented dimensions of the eigenmatrix. Additionally, the finite-difference time-domain method could treat dispersive media elegantly [25] but it was not easy to obtain the complex band structure for lossy media.

In this paper, a novel eigenvalue algorithm is developed to analyze the influence of ohmic (metallic) loss on the complex BS and eigenmodes of plasmonic crystals with arbitrary geometries and materials. The algorithm directly produces a linear eigenequation, and thus saves computer resources in contrast to the QEP. The ohmic loss of plasmonic crystals will modify the group velocity, decay length, quality factor, symmetry and degeneracy of eigenmodes, which are important to diverse practical applications. First, the group velocity governs the transit time per unit transmission length and, thus, the power dissipation of devices. Second, spontaneous decay rate of an atom or molecule is proportional to the quality factor, which is essential to the cavity quantum electrodynamics [26]. Third, symmetry and degeneracy of eigenmodes relate to several fundamental or emerging physical concepts, such as time reversibility [27] and photonic Dirac cones [28]. Consequently, the ohmic loss will affect the performances of slow-wave devices, superlens, cloaking, zero-refractive-index metamaterials, and quantum circuits, which highly depend on the excitation of the fundamental eigenmode or superpositions of few eigenmodes.

2. Method and Theory

In general, BS for any periodic systems can be calculated by the wave equation for either the electric field **E** or the magnetic field **H**. The wave equation for the magnetic field is [1]

$$\nabla \times \frac{1}{\varepsilon(\mathbf{r})} \nabla \times \mathbf{H} = \mu(\mathbf{r}) \left(\frac{\omega}{c}\right)^2 \mathbf{H} \tag{1}$$

where ε and μ are the relative permittivity and relative permeability of the material of interest, **H** is the magnetic field, ω is the frequency, and c is the light speed in vacuum. When the material is dispersive and lossy, ε is complex and is a function of frequency. Otherwise, ε is constant for the nondispersive dielectric material. The nonmagnetic material is assumed here, i.e., $\mu = 1$.

For simplicity and better understanding the principle, we focused on 2-D plasmonic crystals in this paper. In fact, the proposed eigenvalue algorithm can be easily extended to study 3-D plasmonic crystals. For a 2-D periodic system, the object is periodic along the x- and y-directions; and is homogeneous in the z-direction. The electromagnetic fields can be split into a transverse magnetic wave $(\mathrm{TM}_z : E_z, H_x, H_y)$ and a transverse electric wave $(\mathrm{TE}_z : H_z, E_x, E_y)$. Take TE_z mode as an example, the wave equation (1) degenerates to the following scalar wave equation:

$$\frac{\partial}{\partial x}\left(\frac{1}{\varepsilon(x,y)}\frac{\partial H_z}{\partial x}\right) + \frac{\partial}{\partial y}\left(\frac{1}{\varepsilon(x,y)}\frac{\partial H_z}{\partial y}\right) + k_0^2 H_z = 0 \tag{2}$$

where H_z is the magnetic field and $k_0 = (\omega/c)$ is the wavenumber in free space. An $\exp(j\omega t)$ time-dependence is implicit through the paper with t is the time and $j = \sqrt{-1}$. Applying the finite-difference method, the unit cell is divided into many rectangular grids. The geometry is periodic in the transverse (in-plane) directions with lattice constants P_x and P_y. A unit cell with $N\Delta \times N\Delta$ grid points is illustrated in Fig. 1. $\varphi_{m,n}$ $(m, n = 1, 2, 3, \ldots, N)$ denote the magnetic field H_z. The common point of four adjacent grids (rectangles) is a central node connected with its adjacent ones through a five-point finite-difference equation. Regarding the central node at the periodic boundary, some adjacent nodes are out of the unit cell; and can be treated by the periodic boundary conditions

$$\varphi(x \pm P_x, y \pm P_y) = \varphi(x, y)\exp(\mp jk_x P_x \mp jk_y P_y) \tag{3}$$

in which $\exp(jk_x P_x)$ and $\exp(jk_y P_y)$ is the periodic coefficients.

Applying the five-point difference equation and (3), based on the finite-difference grids as shown in Fig. 1, the corresponding discretized form of (2) is given by

$$\begin{pmatrix} \mathcal{M}_{11} & \mathcal{M}_{12} & \{0\}_{N\times N} & \cdots & \{0\}_{N\times N} & \mathcal{M}_{1N}\exp(-jk_x P_x) \\ \mathcal{M}_{21} & \mathcal{M}_{22} & \mathcal{M}_{23} & \cdots & \{0\}_{N\times N} & \{0\}_{N\times N} \\ \{0\}_{N\times N} & \mathcal{M}_{32} & \mathcal{M}_{33} & \mathcal{M}_{34} & \cdots & \{0\}_{N\times N} \\ \vdots & \vdots & \vdots & \vdots & \vdots & \vdots \\ \mathcal{M}_{N1}\exp(jk_x P_x) & \{0\}_{N\times N} & \{0\}_{N\times N} & \cdots & \mathcal{M}_{N(N-1)} & \mathcal{M}_{NN} \end{pmatrix} \psi = 0 \tag{4}$$

where $\psi = (\varphi_{11}\ \varphi_{21}\ \varphi_{31}\ \cdots\ \varphi_{N1}\ \varphi_{12}\ \varphi_{22}\ \varphi_{32}\ \cdots\ \varphi_{N2}\ \cdots\ \varphi_{1N}\ \varphi_{2N}\ \varphi_{3N}\ \cdots\ \varphi_{NN})'$ is the eigenmode, and $\mathcal{M}_{nn}$ and $\mathcal{M}_{mn}(m \neq n)$ are defined as follows:

$$\mathcal{M}_{nn} = \begin{pmatrix} D_{1n} & -T_{2n} & 0 & \cdots & 0 & -T_{Nn}\exp(-jk_y P_y) \\ -T_{1n} & D_{2n} & -T_{3n} & \cdots & 0 & 0 \\ 0 & -T_{2n} & D_{3n} & -T_{4n} & \cdots & 0 \\ \vdots & \vdots & \vdots & \vdots & \vdots & \vdots \\ -T_{1n}\exp(jk_y P_y) & 0 & 0 & \cdots & -T_{(N-1)n} & D_{Nn} \end{pmatrix} \tag{5}$$

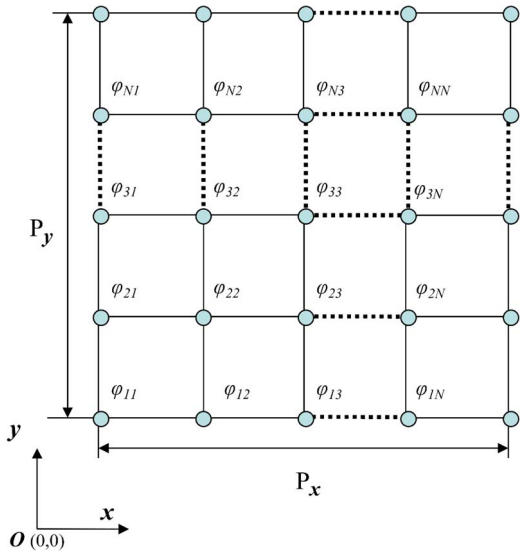

Fig. 1. Unit cell of plasmonic crystals with finite-difference grids.

where $D_{mn} = (2/(\varepsilon_{mn} \cdot \Delta x^2)) + (2/(\varepsilon_{mn} \cdot \Delta y^2)) - k_0^2$, and $T_{mn} = (1/(\varepsilon_{mn} \cdot \Delta y^2))$ for $m = 1, 2, 3, \ldots, N$. Δx and Δy are the spatial steps in the x-direction and y-direction, respectively

$$\mathcal{M}_{mn} = -\frac{1}{\Delta x^2}\begin{pmatrix} \frac{1}{\varepsilon_{1n}} & 0 & 0 & \cdots & 0 \\ 0 & \frac{1}{\varepsilon_{2n}} & 0 & \cdots & 0 \\ 0 & 0 & \frac{1}{\varepsilon_{3n}} & \cdots & 0 \\ \vdots & \vdots & \vdots & \vdots & \vdots \\ 0 & 0 & 0 & \cdots & \frac{1}{\varepsilon_{Nn}} \end{pmatrix}. \tag{6}$$

We define two new matrices $\mathcal{H}$ and $\mathcal{P}$ as

$$\mathcal{H} = \begin{pmatrix} \{0\}_{N\times N} & \{0\}_{N\times N} & \{0\}_{N\times N} & \cdots & \{0\}_{N\times N} & \mathcal{M}_{1N} \\ \mathcal{M}_{21} & \mathcal{M}_{22} & \mathcal{M}_{23} & \cdots & \{0\}_{N\times N} & \{0\}_{N\times N} \\ \{0\}_{N\times N} & \mathcal{M}_{32} & \mathcal{M}_{33} & \mathcal{M}_{34} & \cdots & \{0\}_{N\times N} \\ \vdots & \vdots & \vdots & \vdots & \vdots & \vdots \\ \{0\}_{N\times N} & \{0\}_{N\times N} & \{0\}_{N\times N} & \cdots & \mathcal{M}_{N(N-1)} & \mathcal{M}_{NN} \end{pmatrix} \tag{7}$$

$$\mathcal{P} = -\begin{pmatrix} \mathcal{M}_{11} & \mathcal{M}_{12} & \{0\}_{N\times N} & \cdots & \{0\}_{N\times N} & \{0\}_{N\times N} \\ \{0\}_{N\times N} & \{0\}_{N\times N} & \{0\}_{N\times N} & \cdots & \{0\}_{N\times N} & \{0\}_{N\times N} \\ \{0\}_{N\times N} & \{0\}_{N\times N} & \{0\}_{N\times N} & \cdots & \{0\}_{N\times N} & \{0\}_{N\times N} \\ \vdots & \vdots & \vdots & \vdots & \vdots & \vdots \\ \mathcal{M}_{N1} & \{0\}_{N\times N} & \{0\}_{N\times N} & \cdots & \{0\}_{N\times N} & \{0\}_{N\times N} \end{pmatrix}. \tag{8}$$

Then, (4) can be rewritten as

$$\mathcal{H}\psi = \exp(jk_x P_x)\mathcal{P}\psi. \tag{9}$$

For a given frequency ω and a fixed complex k_y, if the matrix $\mathcal{H}$ or $\mathcal{P}$ can be inverted, (9) will be a normal eigenvalue problem. Unfortunately, the matrix $\mathcal{P}$ obviously cannot be inverted because one of its columns is filled with zeros. Meanwhile, the matrix $\mathcal{H}$ is also singular.

This deficiency can be removed by modifying (9), and then, a linear eigenvalue equation is obtained as

$$(\mathcal{H}-\mathcal{P})\psi = [\exp(jk_xP_x)-1]\mathcal{P}\psi$$
$$(\mathcal{H}-\mathcal{P})^{-1}\mathcal{P}\psi = \frac{1}{\exp(jk_xP_x)-1}\psi. \tag{10}$$

The matrix $(\mathcal{H}-\mathcal{P})$ can always be inverted because its elements are the finite-difference coefficients of the wave equation (2). Once (10) is solved, $\lambda = 1/(\exp(jk_xP_x)-1)$ can be obtained as an eigenvalue, and then the corresponding complex k_x can be solved by $k_x = \log((1/\lambda)+1)/(jP_x)$. The BS of a periodic nanostructure can be obtained by solving the complex k_x via scanning the frequency ω and complex k_y. Alternatively, we can solve the complex k_y via scanning the frequency ω and complex k_x.

For an arbitrary direction in the reciprocal space, in literatures [23], [24], the direction of the Bloch wave vector $\mathbf{k}$ is fixed, and the complex amplitude is calculated as an eigenvalue. Regarding the proposed method, the fixed Bloch wavenumber k_x or k_y is a complex number. Most importantly, the developed eigenvalue algorithm is able to expand the excitation solution in terms of eigenmodes with a significant physical meaning. Considering an inhomogeneous plane wave with a complex wave vector $\mathbf{k}^c_{\text{inc}} = k^c_{ix}\mathbf{e}_x + k^c_{iy}\mathbf{e}_y$ incident on a 2-D finite periodic structure, the bulk excitation solution can be expanded as

$$H_z(\mathbf{r}, \mathbf{k}^c_{\text{inc}}; \omega) = \sum_n A_n\psi_n(\mathbf{r}, k_x, k_{yn}; \omega)|_{k_x=k^c_{ix}} + \sum_n B_n\psi_n(\mathbf{r}, k_{xn}, k_y; \omega)|_{k_y=k^c_{iy}} \tag{11}$$

where ψ_n are the eigenmodes and ω is also complex. The first and second summation terms correspond to the generalized phase (momentum) matching conditions [29] respectively for the horizontal (top/bottom) and vertical (left/right) interfaces. A mode conversion from the incident inhomogeneous plane wave to the excited bulk Bloch wave can be easily understood according to the generalized phase matching conditions.

In general, there are two cases for eigenvalue analysis. On the one hand, it's convenient for the research about wave propagation, when solution is with a real frequency but a complex wave vector. On the other hand, for the research about resonant cavities, the solution with a real wave vector but a complex frequency is more useful. Both cases are all right for different occasions. And the imaginary part of the wave vector gives the spatial domain decay rate. The imaginary part of the frequency gives the decay rate of the eigenstate or, in other words, the inverse of the imaginary part gives the lifetime of the eigenstate.

Although the proposed method allows to calculate all the complex modes via scanning the complex k_x and complex k_y, one could adopt an interpolation method to obtain the band structure with only scanning the real k_x and real k_y, which saves considerable calculation time. Mathematically, we have

$$\omega\left(k^c_x, k^c_y\right) = \sum_n C_n\left(k^c_x, k^c_y; k^r_x, k^c_{yn}\right)\omega_n\left(k^r_x, k^c_{yn}\right)|_{k^r_x=\Re(k^c_x)} + \sum_n D_n\left(k^c_x, k^c_y; k^c_{xn}, k^r_y\right)\omega_n\left(k^c_{xn}, k^r_y\right)|_{k^r_y=\Re(k^c_y)} \tag{12}$$

where c and r denote the complex and real numbers, respectively. C_n and D_n are the interpolation (extrapolation) kernels.

3. Numerical Results

To validate the theoretical model of Section 2, numerical examples are presented in this section. First, a 2-D square-lattice photonic crystal with a lossless dielectric material is considered. The BS along $\Gamma - X$, $X - M$, $M - \Gamma$ is calculated by the proposed algorithm and is compared with the BS calculated by the traditional $\omega = \omega(\mathbf{k})$ approach. Next, we apply the proposed eigenvalue

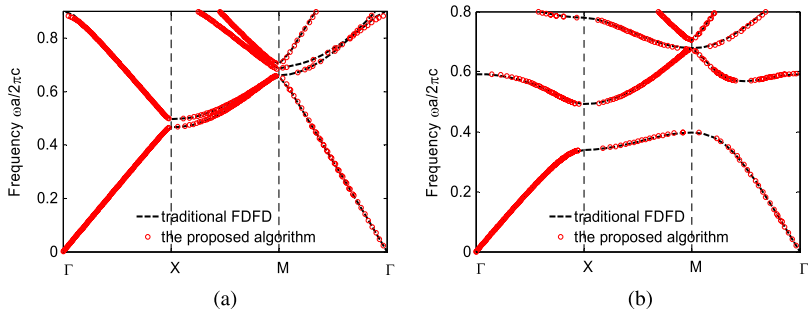

Fig. 2. BS of a 2-D square-lattice photonic crystal with GaAs square in the background of air. The permittivity of GaAs is 11.56, and the square side is 0.2*a* (*a* is lattice constant). The black lines represent the results calculated by the traditional $\omega = \omega(\mathbf{k})$ approach, while the red circles denote the results obtained by proposed $\mathbf{k} = \mathbf{k}(\omega)$ algorithm. (a) TE_z mode. (b) TM_z mode.

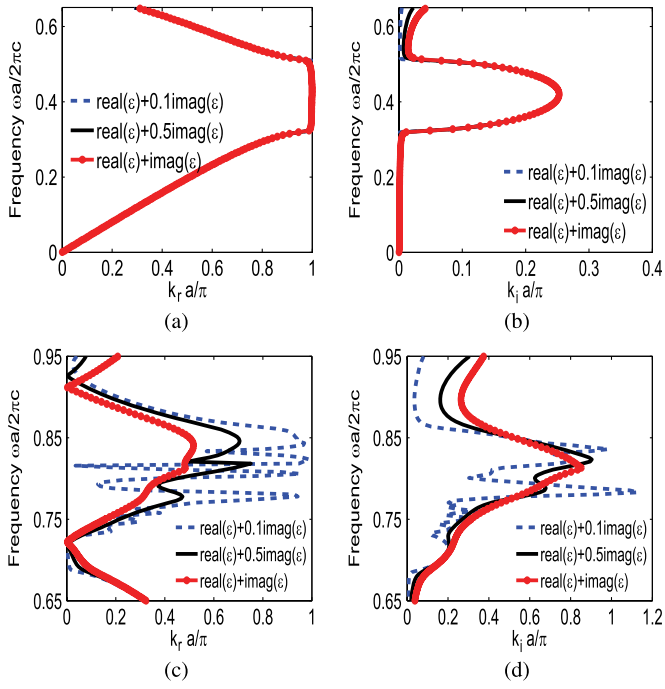

Fig. 3. Band structures of a 2-D square-lattice plasmonic crystal obtained by the proposed method with silver cylinders in the background of air. TE_z polarization is considered. The complex permittivity of silver is expressed by the Brendel-Bormann model. The radius of the metal cylinder is 0.3*a* (*a* is the lattice constant). Each color represents a result with different imaginary part of primitivity of the silver. (a) Real part and (b) the imaginary part of the Bloch wavenumber with the normalized frequency below 0.65. (c) Real part and (d) the imaginary part of the Bloch wavenumber with the normalized frequency between 0.65 and 0.95.

algorithm to plasmonic crystals and investigate the influence of loss on the complex BS and eigenmodes. It should be noted that all of BS results below are drawn with the normalized frequency $(\omega a/2\pi c)$.

3.1. Dielectric Photonic Crystals

We consider a 2-D square-lattice photonic crystal comprising square dielectric rods in the background of air. $P_x = P_y = a$ are the lattice constants, and the square length is 0.2*a*. The permittivity of each dielectric rod is 11.56 corresponding to the dielectric constant of GaAs in the optical frequency regime. Band structures are calculated by our algorithm for both TE_z and TM_z

TABLE 1

Quality Factor Q for TE_z

Q	$\mathrm{Re}(\varepsilon)+j\mathrm{Im}(\varepsilon)$	$\mathrm{Re}(\varepsilon)+0.1j\mathrm{Im}(\varepsilon)$
$\frac{\omega a}{2\pi c} = 0.323$	20.129	20.747
$\frac{\omega a}{2\pi c} = 0.433$	3.987	3.987
$\frac{\omega a}{2\pi c} = 0.509$	14.553	16.836

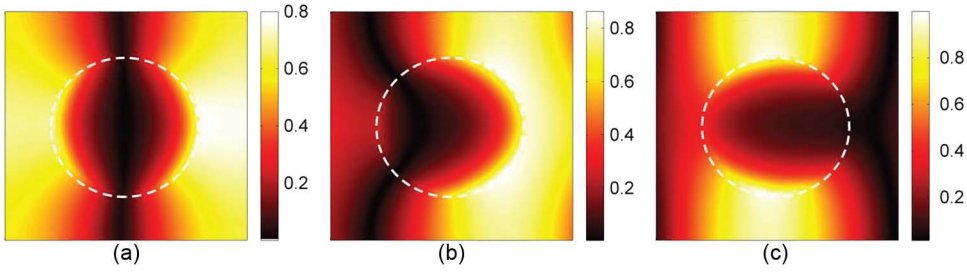

Fig. 4. H_z field distribution obtained by the proposed algorithm for TE_z mode with $\mathrm{Re}(\varepsilon)+j\mathrm{Im}(\varepsilon)$. (a) Normalized frequency 0.323 corresponding to the lower band edge. (b) Normalized frequency 0.433 corresponding to the band gap. (c) Normalized frequency 0.509 corresponding to the upper band edge.

modes, respectively, corresponding to Fig. 2(a) and (b). The validity of our algorithm is confirmed by comparing to the results from the traditional $\omega = \omega(\mathbf{k})$ approach with the same finite-difference grids. As shown in Fig. 2, both methods agree with each other well.

3.2. Plasmonic Crystals

The second example is a PC that consists of a 2-D square array of infinite metallic cylinders in air. The complex permittivity of metal (silver) is expressed by the Brendel-Bormann model [30]. The lattice length of the unit cell is set to be $a = 280$ nm and the radius of the metal cylinder is $r = 0.3a$.

Using the proposed algorithm, the BS for TE_z polarization along the $\Gamma - X$ direction is presented in Fig. 3. In order to study the influence of the loss on the BS and eigenmodes, we gradually decrease the imaginary part of primitivity of the metal, i.e., $\mathrm{Re}(\varepsilon)+j\mathrm{Im}(\varepsilon)$, $\mathrm{Re}(\varepsilon)+0.5j\mathrm{Im}(\varepsilon)$ and $\mathrm{Re}(\varepsilon)+0.1j\mathrm{Im}(\varepsilon)$. Here, $\mathrm{Re}(\varepsilon)+j\mathrm{Im}(\varepsilon)$ is the physically real value of the permittivity by the Brendel-Bormann model.

3.2.1 Case (a): TE_z Polarization

As depicted in Fig. 3(a) and (b), the ohmic (metallic) loss does not strongly modify the BS when the normalized frequency is below 0.65 for both real part k_r and imaginary part k_i of the Bloch wavenumber. Table 1 lists the quality factors of eigenmodes defined as k_r/k_i. A large ohmic loss induces a low quality factor especially at high frequencies. Moreover, we can observe a plasmonic bandgap with a large attenuation coefficient k_i [see Fig. 3(b)] and two plasmonic band edges with near zero group velocity [see Fig. 3(a)]. The corresponding eigenmode distributions at the bandgap and band edges are presented in Fig. 4. Interestingly, H_z field shows different concentration regions respectively along x and y directions at the two band edges. Because $k_r > k_0$ and $k_r < k_0$ are respectively satisfied at the lower band edge and upper one. When the normalized frequency approaches the plasmonic resonance frequency, the drastic oscillations of the BS can be observed at Fig. 3(c) and (d) for the low ohmic loss. As the ohmic loss boosts, the plasma oscillation is damped and thus BS becomes smooth. Next we investigate the eigenmodes around the plasmonic resonance frequency as illustrated in Fig. 5, the field confinement of eigenmodes is remarkably enhanced as the ohmic loss decreases.

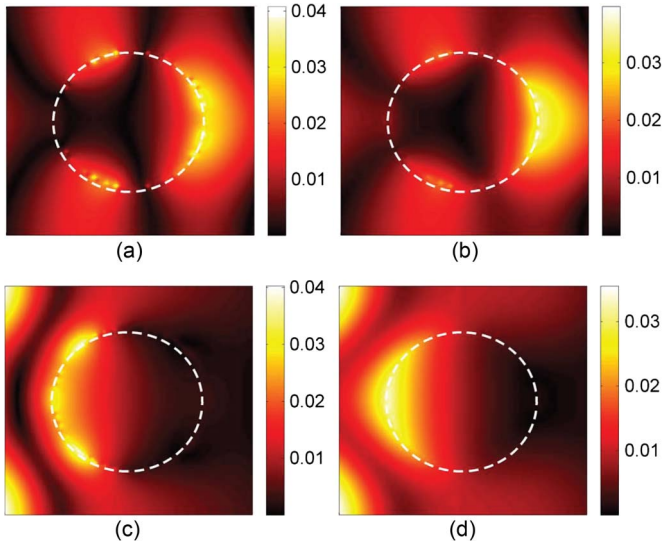

Fig. 5. H_z field distribution obtained by the proposed algorithm for TE_z mode. (a), (b) Normalized frequency 0.723, respectively, with the metal permittivity of $\mathrm{Re}(\varepsilon) + 0.1j\mathrm{Im}(\varepsilon)$ and $\mathrm{Re}(\varepsilon) + j\mathrm{Im}(\varepsilon)$. (c), (d) Normalized frequency 0.841, respectively, with the metal permittivity of $\mathrm{Re}(\varepsilon) + 0.1j\mathrm{Im}(\varepsilon)$ and $\mathrm{Re}(\varepsilon) + j\mathrm{Im}(\varepsilon)$.

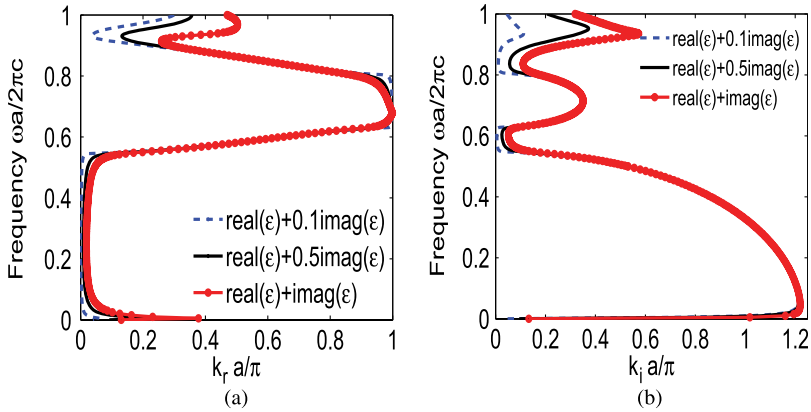

Fig. 6. Band structures of a 2-D square-lattice plasmonic crystal obtained by the proposed method with silver cylinders in the background of air. TM_z polarization is considered. The complex permittivity of silver is expressed by the Brendel-Bormann model. The radius of the metal cylinder is $0.3a$ (a is the lattice constant). Each color represents a result with different imaginary part of primitivity of the silver. (a) Real part and (b) imaginary part of the Bloch wavenumber with the normalized frequency between 0 and 1.

3.2.2 Case (b): TM_z Polarization

Fig. 6(a) and (b) show the BS for TM_z polarization. Particularly, there is a cut-off frequency around $\omega a/2\pi c = 0.533$ below which the waves cannot propagate. Different from TE_z polarization, plasmonic effects cannot be supported at the TM_z polarization. Although the BS has no drastic oscillation regions, photonic bandgap around $\omega a/2\pi c = 0.701$ still opens up due to the Bragg backscattering. At the bandgap in Fig. 6(a), the vertical dispersion curve for the low ohmic loss is distorted and twisted as the ohmic loss becomes increasingly larger. The group velocity $(d\omega/dk_r)$ along the x direction changes the sign at the two band edges, which can be seen from the field distribution of eigenmodes as well (see Fig. 7). From the results listed in Table 2, the

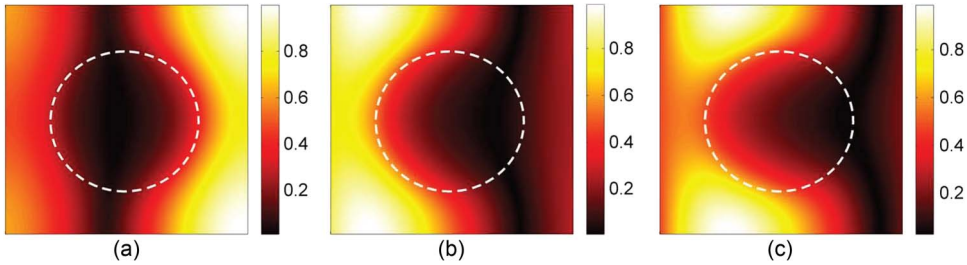

Fig. 7. E_z field distribution obtained by the proposed algorithm for TM_z mode with $\mathrm{Re}(\varepsilon) + i\mathrm{Im}(\varepsilon)$. (a) Normalized frequency 0.636 corresponding to the lower band edge. (b) Normalized frequency 0.701 corresponding to the bandgap. (c) Normalized frequency 0.774 corresponding to the upper band edge.

TABLE 2

Quality Factor Q for TM_z

Q	$\mathrm{Re}(\varepsilon) + j\mathrm{Im}(\varepsilon)$	$\mathrm{Re}(\varepsilon) + 0.1j\mathrm{Im}(\varepsilon)$
$\frac{\omega a}{2\pi c} = 0.636$	6.208	7.005
$\frac{\omega a}{2\pi c} = 0.701$	2.854	2.894
$\frac{\omega a}{2\pi c} = 0.774$	3.448	3.758

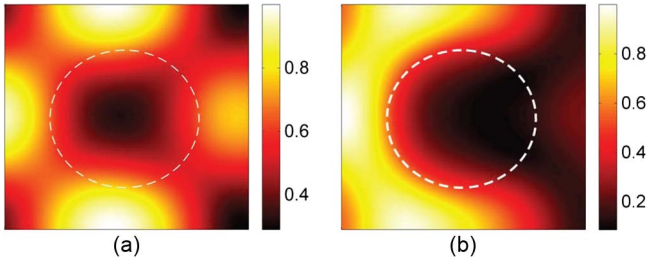

Fig. 8. E_z field distribution obtained by the proposed algorithm for TM_z mode with a normalized frequency 0.965. (a) $\mathrm{Re}(\varepsilon) + 0.1i\mathrm{Im}(\varepsilon)$. (b) $\mathrm{Re}(\varepsilon) + i\mathrm{Im}(\varepsilon)$.

reduced ohmic loss enlarges the quality factor, which is the same as the TE_z wave. Additionally, Fig. 8 shows the eigenmodes at higher frequency where the ohmic loss breaks the symmetry of eigenmodes.

4. Conclusion

A novel eigenvalue algorithm was proposed to study the influence of ohmic loss on the BS and eigenmodes of dispersive plasmonic crystals. For TM_z polarization, the high ohmic loss strongly damps the oscillation of the BS and meanwhile weakens the optical field confinement of eigenmodes around the plasmonic resonance frequency. For TE_z polarization, the high ohmic loss distorts the vertical dispersion curve at the bandgap and breaks the symmetry of eigenmodes. For both polarizations, the small quality factor of the eigenmode is obtained with the large ohmic loss. This work is fundamentally important to the optimized design of plasmonic crystals.

References

[1] J. D. Joannopoulos, S. G. Johnson, J. N. Winn, and R. D. Meada, *Photonic Crystals: Molding the Flow of Light*. Princeton, NJ, USA: Princeton Univ. Press, 2008.
[2] P. Y. Chen, R. C. McPhedran, and C. M. de Sterke, "Group velocity in lossy periodic structure media," *Phys. Rev. A, At. Mol. Opt. Phys. Quantum Inf.*, vol. 82, no. 5, Nov. 2010, Art. no. 053825.

[3] K. Sakoda, *Optical Properties of Photonic Crystals*. Berlin, Germany: Springer-Verlag, 2005.
[4] S. G. Johnson and J. D. Joannopoulos, "Block-iterative frequency-domain methods for Maxwell's equations in a planewave basis," *Opt. Exp.*, vol. 8, no. 3, pp. 173–190, Jan. 2001.
[5] B. P. Hiett *et al.*, "Application of finite element methods to photonic crystal modelling," *Proc. Inst. Elect. Eng.—Sci. Meas. Technol.*, vol. 149, no. 5, pp. 293–296, Sep. 2002.
[6] H. Rather, *Surface Plasmons on Smooth and Rough Surfaces and on Gratings*. Berlin, Germany: Springer-Verlag, 1998.
[7] V. M. Agranovich and D. L. Mills, *Surface Polaritons: Electromagnetic Waves at Surfaces and Interfaces*. Amsterdam, The Netherlands: North-Holland, 1982.
[8] W. E. I. Sha, L. L. Meng, W. C. H. Choy, and W. C. Chew, "Observing abnormally large group velocity at the plasmonic band edge via a universal eigenvalue analysis," *Opt. Lett.*, vol. 39, no. 1, pp. 158–161, Jan. 2014.
[9] D. de Ceglia, M. A. Vincenti, M. Scalora, N. Akozbek, and M. J. Bloemer, "Plasmonic band edge effects on the transmission properties of metal grating," *AIP Adv.*, vol. 1, no. 3, Sep. 2011, Art. no. 032151.
[10] Z. Y. Li, R. J. Liu, L. Gan, J. X. Fu, and J. Lian, "Nonreciprocal electromagnetic devices in gyromagnetic photonic crystals," *Int. J. Mod. Phys. B*, vol. 28, no. 2, Jan. 2014, Art. no. 1441010.
[11] Z. L. Wang, C. T. Chan, W. Y. Zhang, N. B. Ming, and P. Sheng, "Three-dimensional self-assembly of metal nanoparticles: Possible photonic crystal with a complete gap below the plasma frequency," *Phys. Rev. B, Condens. Matter Mater. Phys.*, vol. 64, no. 11, Sep. 2001, Art. no. 113108.
[12] M. Westphalen, U. Kreibig, J. Rostalski, H. Luth, and D. Meissner, "Metal cluster enhanced organic solar cells," *Sol. Energy Mater. Sol. Cells*, vol. 61, no. 1, pp. 97–105, Feb. 2000.
[13] X. H. Li, W. E. I. Sha, W. C. H. Choy, D. D. S. Fung, and F. X. Xie, "Efficient inverted polymer solar cells with directly patterned active layer and silver back grating," *J. Phys. Chem. C*, vol. 116, no. 12, pp. 7200–7206, Mar. 2012.
[14] W. E. I. Sha, W. C. H. Choy, and W. C. Chew, "A comprehensive study for the plasmonic thin-film solar cell with periodic structure," *Opt. Exp.*, vol. 18, no. 6, pp. 5993–6007, Mar. 2010.
[15] Y. Lu, G. L. Liu, J. Kim, Y. X. Mejia, and L. P. Lee, "Nanophotonic crescent moon structures with sharp edge for ultrasensitive biomolecular detection by local electromagnetic field enhancement effect," *Nano Lett.*, vol. 5, no. 1, pp. 119–124, Jan. 2005.
[16] Y. F. Wang *et al.*, "Optical properties of the crescent and coherent applications," *Opt. Exp.*, vol. 19, no. 9, pp. 8303–8311, Apr. 2011.
[17] M. L. Brongersma and P. G. Kik, *Surface Plasmon Nanophotonics*. Dordrecht, The Netherlands: Springer-Verlag, 2007.
[18] J. N. Anker *et al.*, "Biosensing with plasmonic nanosensors," *Nat. Mater.*, vol. 7, no. 6, pp. 442–453, Jun. 2008.
[19] A. O. Korotkevich, X. J. Ni, and A. V. Kildishev, "Fast eigensolver for plasmonic metasurfaces," *Opt. Mater. Exp.*, vol. 4, no. 2, pp. 288–299, Feb. 2008.
[20] A. Raman and S. H. Fan, "Photonic band structure of dispersive metamaterials formulated as a Hermitian eigenvalue problem," *Phys. Rev. Lett.*, vol. 104, no. 8, Feb. 2010, Art. no. 087401.
[21] B. Jiang, Y. J. Zhang, Y. F. Wang, and W. H. Zheng, "Band structure of photonic crystal with dispersive and lossy materials using Dirichlet-to-Neumann wave vector eigen equation method," *J. Appl. Phys.*, vol. 112, no. 3, Aug. 2012, Art. no. 033112.
[22] M. Luo and Q. H. Liu, "Three-dimensional dispersive metallic photonic crystals with a bandgap and a high cutoff frequency," *J. Opt. Soc. Amer. A, Opt. Image Sci.*, vol. 27, no. 8, pp. 1878–1884, Aug. 2010.
[23] M. Davanco, Y. Urzhumov, and G. Shvets, "The complex Bloch bands of a 2D plasmonic crystal displaying isotropic negative refraction," *Opt. Exp.*, vol. 15, no. 15, pp. 9681–9691, Jul. 2007.
[24] C. Fietz, Y. Urzhumov, and G. Shvets, "Complex k band diagrams of 3D metamaterial/photonic crystals," *Opt. Exp.*, vol. 19, no. 20, pp. 19027–19041, Sep. 2011.
[25] M. Qiu and S. L. He, "A nonorthogonal finite-difference time-domain method for computing the band structure of a two-dimensional photonic crystal with dielectric and metallic inclusions," *J. Appl. Phys.*, vol. 87, no. 12, pp. 8268–8275, Jun. 2000.
[26] P. F. Qiao, W. E. I. Sha, W. C. H. Choy, and W. C. Chew, "Systematic study of spontaneous emission in a two-dimensional arbitrary inhomogeneous environment," *Phys. Rev. A.*, vol. 83, no. 4, Apr. 2011, Art. no. 043824.
[27] K. H. Fung, R. C. H. Tang, and C. T. Chan, "Analytical properties of the plasmon decay profile in a periodic metal-nanoparticle chain," *Opt. Lett.*, vol. 36, no. 12, pp. 2206–2208, Jun. 2011.
[28] X. Huang, Y. Lai, Z. H. Hang, H. Zheng, and C. T. Chan, "Dirac cones induced by accidental degeneracy in photonic crystals and zero-refractive-index materials," *Nat. Mat.*, vol. 10, no. 8, pp. 582–586, Aug. 2011.
[29] X. Zhang and S. R. Forrest, "Generalized phase matching condition for lossy periodic photonic structures," *Opt. Exp.*, vol. 18, no. 2, pp. 1151–1158, Jan. 2010.
[30] A. D. Rakic, A. B. Djurisic, J. M. Elazar, and M. L. Majewski, "Optical properties of metallic films for vertical-cavity optoelectronic devices," *Appl. Opt.*, vol. 37, no. 22, pp. 5271–5283, Aug. 1998.